SCIENTIFIC REPORTS

OPEN

SUBJECT AREAS:
QUANTUM OPTICS
NONLINEAR OPTICS

Received
17 October 2013

Accepted
4 April 2014

Published
28 April 2014

Correspondence and requests for materials should be addressed to Y.-Q.L. (yqlu@nju.edu.cn) or F.X. (feixu@nju.edu.cn)

Tailoring entanglement through domain engineering in a lithium niobate waveguide

Yang Ming[1,3], Ai-Hong Tan[2], Zi-Jian Wu[1,3], Zhao-Xian Chen[1,3], Fei Xu[1,3] & Yan-Qing Lu[1,3]

[1]National Laboratory of Solid State Microstructures and College of Engineering and Applied Sciences, Nanjing University, Nanjing 210093, China, [2]Laboratory for Quantum Information, China Jiliang University, Hangzhou 310018, China, [3]National Center of Microstructures and Quantum Manipulation, Nanjing University, Nanjing 210093, China.

We propose to integrate the electro-optic (EO) tuning function into on-chip domain engineered lithium niobate (LN) waveguide. Due to the versatility of LN, both the spontaneously parametric down conversion (SPDC) and EO interaction could be realized simultaneously. Photon pairs are generated through SPDC, and the formation of entangled state is modulated by EO processes. An EO tunable polarization-entangled photon state is proposed. Orthogonally-polarized and parallel-polarized entanglements of photon pairs are instantly switchable by tuning the applied field. The characteristics of the source are theoretically investigated showing adjustable bandwidths and high entanglement degrees. Moreover, other kinds of reconfigurable entanglement are also achievable based on suitable domain-design. We believe tailoring entanglement based on domain engineering is a very promising solution for next generation function-integrated quantum circuits.

Entanglement is a crucial physical resource for quantum information science and technology. In practical investigations and applications, entanglement systems based on photons are widely used owing to the extra long decoherence time. To perform various specific tasks, different kinds of entanglements are required, such as multi-particle entanglement, nonmaximally entanglement, and mixed state entanglement[1–7]. For the generation of entangled photons, spontaneous parametric down conversion (SPDC) in $\chi^{(2)}$ nonlinear crystals is one of the most powerful tools[8]. In SPDC process, a single photon is transformed into a photon pair. However, in previous works[1–4], it is usually necessary to design complicated optical paths to transform the initially generated states into target entangled states. Numerous large-scale bulk optical elements have to be fixed onto sizeable optical benches in the laboratory, such as lenses, wave plates and filters[9,10]. The physical size and the inherent instability of these components hinder the development of more complex schemes, and bring significant challenges for the integration of quantum circuits, which needs to be improved in practical applications[11,12].

In this article, we propose a different strategy for on-chip tailoring entanglement through domain engineering in a lithium niobate (LN) waveguide. LN is a typical ferroelectric nonlinear optical material, which is simultaneously available for SPDC[13] and electro-optic (EO) effect[14–16]. Due to its quite large effective nonlinear coefficient, LN could serve as entangled photon-pair source of high quality[17,18]. What's more, EO modulation is an effective way to manipulate entangled photons. Previous investigations have demonstrated the control of phase[19] or polarization state[14]. An integrated quantum relay operator has been established based on EO effect of single domain LN crystals with some special electrode design[15]. In fact, at the quantum level, EO could be regarded as a two-photon interaction process, in which the quantum states of photons could exchange. In this work, we derive relevant theories to describe this process. Combining the theories for EO and SPDC, entangled states of desired formations could be designed flexibly. Through suitable domain engineering, which is widely used in quasi phase matching (QPM) nonlinear optics[9], the EO and SPDC processes could be effectively combined to generate the needed entangled states. Moreover, LN is also a good platform to realize versatile functions including efficient infrared photon detection[20], negative permittivity[21], EO quantum logic gate[22] and lensless ghost imaging[23]. All of them could be integrated together toward future practical large scale quantum circuit integration.

Following, as an illustration of our entanglement design approach, we establish an EO tunable polarization-entangled photon pair source in a domain engineered LN waveguide with suitable artificial structures. When a suitable voltage is applied, the source produces a pair of entangled photons contains the same polarization, with either o- or e- polarization state. The notations o- and e- represent ordinary and extraordinary light in uniaxial

anisotropy crystal, respectively. In contrast, if the voltage is turned off, the entangled photons bear orthogonal polarization states, i.e., one photon is o-polarized while another one has e-polarization. Since we may control the polarization state intentionally, the formations of entangled states thus could be regulated accordingly, which possess considerable potential in modulation of multi-photon entangled states.

Results

Tailoring entanglement in a domain engineered LN waveguide. In recent works[24–26], integrated quantum circuits established on silicon waveguides are adequately investigated. Utilizing the femtosecond laser waveguide writing technology, on-chip devices to support and manuscript polarization-encoded qubits have been fabricated[27,28]. A controlled-NOT gate has been experimental demonstrated with switchable entanglement. It is no doubt that silicon waveguides have excellent capabilities to confine and propagate light. However, limited by the inherent properties of silicon, they are not very convenient for fast manipulating and modulating entangled photons; such as the modulation scheme based on thermo-optical effect[25], the response time still has much room to improve in practical applications. In addition, to realize multifunctional integrated quantum circuits, entanglements of complicated formations are normally required such as the nonmaximally entanglement[3,5] and mixed state entanglement[4,6,7]. Under these circumstances, the LN-based system is considered as an alternative choice. Besides excellent nonlinear optical properties, EO effect in LN material provides an effective way to change the quantum state of photons through the photon interaction process. For a LN crystal, if we set its symmetry axis as the z-axis and apply a voltage along the y-axis, a variation is led into the dielectric constant. It could be written as $\varepsilon = \varepsilon(0) + \Delta\varepsilon$ with $\Delta\varepsilon_{jk} = -\varepsilon_0\gamma_{51}E_a n_o^2 n_e^2$ $(jk = 23, 32)$[16]. In the equation, γ_{51} is the effective EO coefficient, and E_a represents the applied electric field. The refractive indices of ordinary and extraordinary light are marked as n_o and n_e. This additional portion of permittivity corresponds to an equivalent polarization item, which is expressed as $P_j = -\sum_k \varepsilon_0\gamma_{51}E_a n_o^2 n_e^2 \Delta_{jk}E_k$ with $\Delta_{jk} = \begin{cases} 1, & jk = (23, 32) \\ 0, & else \end{cases}$. From $H_I = \frac{1}{2}\int_V d^3r P\cdot E$, we obtain the interaction Hamiltonian for EO process as

$$H_I = \frac{\hbar\varepsilon_0\gamma_{51}E_a}{4}\Big[\int_{-L}^{0} dx f(x)e^{i(\beta_e-\beta_o)x}\iint d\omega d\omega' F_{EO}\sqrt{\frac{\omega\omega' n_o^2 n_e^2}{N_o N_e}}a_o^\dagger a_e e^{-i(\omega-\omega')t} + \int_{-L}^{0} dx f(x)e^{i(\beta_o-\beta_e)x}\iint d\omega d\omega' F_{EO}\sqrt{\frac{\omega\omega' n_o^2 n_e^2}{N_o N_e}}a_e^\dagger a_o e^{-i(\omega'-\omega)t}\Big] \quad (1)$$

with

$$F_{EO} = \iint dydz\,\vartheta_o(\vec{r})\vartheta_e(\vec{r}). \quad (2)$$

In the equation, the quantized expression of electric field is utilized. F_{EO} is the overlap integral of waveguide modes expressed as $\vartheta(\vec{r})$. The function $f(x)$ represents the structures of the inverted domains. The EO coefficient is periodically modulated, thus the o- and e-beams are coupled due to the periodic index ellipsoid deformation. The phase matching condition should be satisfied between the ordinary and extraordinary photons to ensure high conversion efficiency. The first item of the equation represents the annihilation of an e-polarized photon and the creation of an o-polarized photon, while the second corresponds to the inverse process. Accompanied by the two photon interaction process, the old photon state is substituted by new state which is desired to form target entangled state. Choosing proper EO processes to modulate entangled photon states supplies an innovative approach for entanglement architectures.

As a simple illustration, the polarization qubit of photon is considered. Assuming H_I is acted on a photon with polarization state $|o\rangle$, it would be transformed into polarization state $|e\rangle$ with a certain possibility. Referring to the corresponding classical situation[16], we could obtain a superposition of $|o\rangle$ and $|e\rangle$ through modulating the applied voltage. The ratio of these two portions is determined by the value of applied voltage. The overall effect could be equivalent to $H_{EO} = R(\alpha)H_I$, where R is a standard rotation operator, and α is the equivalent rotation angle. For a biphoton state, the modulation process could be written as

$$|\Psi_f\rangle = H_{EO1}\otimes H_{EO2}|\Psi_i\rangle \quad (3)$$

with the matrix expression of the operator as

$$\begin{bmatrix} \sin\theta\sin\phi & -\sin\theta\cos\phi & -\cos\theta\sin\phi & \cos\theta\cos\phi \\ -\sin\theta\cos\phi & -\sin\theta\sin\phi & \cos\theta\cos\phi & \cos\theta\sin\phi \\ -\cos\theta\sin\phi & \cos\theta\cos\phi & -\sin\theta\sin\phi & \sin\theta\cos\phi \\ \cos\theta\cos\phi & \cos\theta\sin\phi & \sin\theta\cos\phi & \sin\theta\sin\phi \end{bmatrix}, \quad (4)$$

where θ and φ are the corresponding equivalent rotation angles to determine the relative ratio of the two photon vector states, which are controlled by the applied voltage. It works similar to a half waveplate (HWP). However, there are still apparent differences. Assuming the input light is a linearly polarized light, a circular polarized beam is obtained if the wave plate thickness is only half. In contrast, the light passing through a PPLN with half-length is still linear-polarized, while the orientation angle is also half if the applied field is the same.

For universal multiphoton entangled state, they could not be generated through SPDC directly, so the postprocessing modulations are quite critical. In multiphoton entanglement situation, only certain formations may lead to potential applications. We need to choose proper photons from the initial state $F\{|\Psi_1\rangle; |\Psi_2\rangle\cdots\cdots|\Psi_N\rangle\}$, where $\{|\Psi_n\rangle\}$ represents the photon pairs from SPDC, and the function $F(|\Psi\rangle)$ corresponds to their initial combination formation. After suitable modulations are applied based on the effective H_{EO}, the state thus could be transformed into a valuable formation such as GHZ state or cluster state. This process could be expressed as

$$|\Psi_f\rangle = \bigotimes_{|\Psi_{k_i}\rangle\in\{|\Psi_n\rangle\}}^{k_N} H_{EO}^{k_i} F\{|\Psi_1\rangle; |\Psi_2\rangle\cdots\cdots|\Psi_N\rangle\}, \quad (5)$$

where $\otimes$ refers to the direct product of all $H_{EO}^{k_i}$.

After the corresponding scheme is decided, the ferroelectric domains of the LN waveguide could be well-designed to satisfy the phase matching conditions of the related SPDC and EO processes. Through analyses of the set of $\{\Delta k_n\}$, the matching vectors could be obtained as $\{2\pi/\Lambda_m\}$. Accordingly, the corresponding Fourier coefficients and the Fourier bases could be derivate. Based on these, the original function is recovered through

$$f(\vec{r}) = \sum_m F_m e^{iK_m\cdot\vec{r}}, \quad (6)$$

where $f(r)$ represents the actual domain arrangement of the entangled photon-pair source. It is worth mentioning that the correspondence between $\{\Delta k_n\}$ and $\{2\pi/\Lambda_m\}$ does not have to be one-to-one. The choice of $\{\Lambda_m\}$ is flexible, which is an important part of domain engineering.

EO tunable polarization-entangled photon state. As a detailed illustration, we consider the generation of an EO tunable polarization-entangled photon state with switchable characteristic. We consider the processes of photon interactions in a z-cut, x-propagating titanium in-diffused LN waveguide. There are well defined transverse electric (TE) and transverse magnetic (TM)

propagation modes in the waveguide at near-infrared frequencies[29]. In this work, only the fundamental modes of the TE and TM modes are discussed. For convenience, they are marked as o-polarized and e-polarized, respectively[30]. Three photon interaction processes are included. They are two SPDC processes, which are expressed as $o_p \rightarrow o_s + e_i$, $o_p \rightarrow e_s + o_i$ (p, s, and i represent the pump, signal, and idler waves. o and e correspond to ordinary and extraordinary polarization); and an EO process takes place for the signal wave, namely $o_s \rightarrow e_s$ ($e_s \rightarrow o_s$). If there is no voltage applied, only the SPDC processes happen in the waveguide. The power of the pump light is launched into the downconversion photons in corresponding propagation modes of the waveguide, the generated entangled state is type-II-like with the formation $|o_s,e_i\rangle + |e_s,o_i\rangle$. In contrast, if there is an applied voltage, the EO effect is activated. The EO polarization rotation and SPDC processes happen simultaneously and are coupled everywhere in the crystal. In this case, the down-converted photons are equally generated everywhere and affected by the locally EO perturbed refractive index ellipsoid. The final obtained polarization state, including, e_s, o_i, e_i and o_s are the superposition result of all "sub-sources" inside the crystal. Therefore the rotation of polarization is realized through coherent superposition of all kinds of photons randomly collected in the sample. Corresponding to the coupling wave theory, that means the power of the fundamental TE mode (o_s) and the TM mode (e_s) at the signal frequency exchanges with each other. For a given sample length, the efficiency is dependent on the interaction strength, which is proportionate to the applied voltage. We could always find a proper voltage to make the efficiency reach ~100%, then the entangled state is switched to be type-I-like with the formation $|e_s,e_i\rangle + |o_s,o_i\rangle$. Thus the entangled state is switchable through controlling the applied voltage on and off.

To satisfy phase matching conditions of the three interaction processes, the domain structures need to be well designed. General speaking, we may design three sets of domain periods so that their reciprocal vectors are able to compensate these three wave vector mismatches. However, this straightforward scheme normally induces very thin domains and complicated structures. To solve this problem, several approaches have been proposed. For example, for the optimized wavelengths and domain structures, the needed domain periods could be reduced to two and they are of integer ratio, so that the domain structure could be easily fabricated. The schematic is shown in Fig. 1. Correspondingly, the sign of nonlinear coefficient $\chi^{(2)}$ and EO coefficient γ change periodically. The modulation functions are expressed as $d(x) = d_{31}f_1(x)f_2(x)$ and $\gamma(x) = \gamma_{51}f_1(x)f_2(x)$[30], where $f(x) = sign[cos(2\pi/\Lambda)] = \Sigma_m G_m exp(ik_m x)$. In the equations, d is the substitute of nonlinear coefficient $\chi^{(2)}$ with the relationship $d = \chi^{(2)}/2$. The effective component of d and γ in our situation are d_{31} and γ_{51}, respectively. Thus the reciprocal vectors are given as $k_m = 2m\pi/\Lambda$, with their corresponding Fourier coefficients as $G_m = (2/m\pi)sin(m\pi/2)$. As a consequence, the expansion formulation of the coefficients are obtained as[31]

$$d(x) = d_{31}\sum_{m,n} G_{m,n}e^{iK_{m,n}x}$$
$$\gamma(x) = \gamma_{51}\sum_{m,n} G_{m,n}e^{iK_{m,n}x} \quad (7)$$

with

$$G_{m,n} = \frac{4}{mn\pi^2}\sin\left(\frac{m\pi}{2}\right)\sin\left(\frac{n\pi}{2}\right)$$
$$K_{m,n} = \frac{2m\pi}{\Lambda_1} + \frac{2n\pi}{\Lambda_2}, \quad (8)$$

where Λ_1 and Λ_2 represents the corresponding two modulation periods. Based on these analyses, the equations of QPM conditions could be expressed as

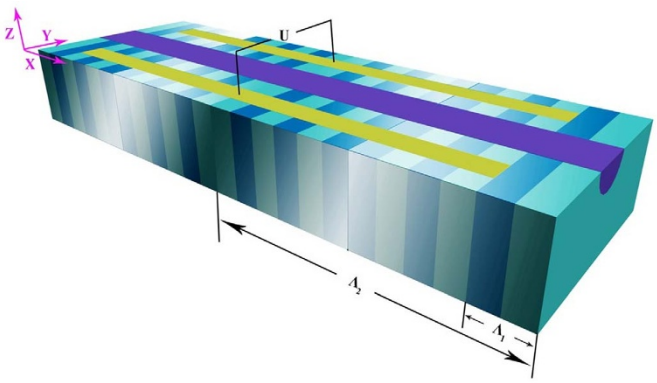

Figure 1 | Schematic of a dual-PPLN waveguide. The light and dark blue portions represent the positive and negative domains of the PPLN, respectively; while the purple portion is the core of the waveguide. The two golden strips correspond to the electrodes. Λ_1 and Λ_2 are the two periods of the structure. Moreover, the polarization directions of o- and e-polarized photons are corresponding to y- and z-directions, respectively.

$$\Delta\beta_1 = \beta_{p,o} - \beta_{s,o} - \beta_{i,e} = K_{m_1,n_1}$$
$$\Delta\beta_2 = \beta_{p,o} - \beta_{s,e} - \beta_{i,o} = K_{m_2,n_2}. \quad (9)$$
$$\Delta\beta_3 = \beta_{s,o} - \beta_{s,e} = K_{m_3,n_3}$$

In these equations, $\beta_{j,\sigma}$ (j = p, s, i; σ = o, e) refers to the propagation constant of the corresponding waveguide mode, which is obtained based on the Hermite-Gauss formulations[29]. $\Delta\beta_1$ and $\Delta\beta_2$ correspond to two SPDC processes, while $\Delta\beta_3$ corresponds to the EO interaction. Km_i,n_i (i = 1, 2, 3) are the required reciprocal vectors to compensate the phase mismatches.

Through detailed calculations, we find an appropriate set of solutions for Eq. (9). The width and depth of the waveguide core are both set at 10 μm, and the maximum of index difference is set at 0.003. The pump, signal and idler wavelengths are 0.7335 μm, 1.6568 μm and 1.3162 μm, respectively. As room temperature operation is always more appreciated for future quantum circuits, the simulation temperature is chosen at 25°C. The photorefractive effect might bring some influences. However, the photorefractive damage of LN is not a simple process. It depends on many factors such as laser pulse width, operation wavelength and surface quality. Through recent technologies[32], the damage threshold has been increased to an acceptable degree for many applications. Moreover, the MgO doping is also an effective way to further avoid crystal damage[33,34]. In this situation, the corresponding values for the (m, n) series are $\{(m_1, n_1) = (3, 1), (m_2, n_2) = (3, -1), (m_3, n_3) = (1, 1)\}$. The dual-modulation periods are obtained at $\Lambda_1 = 25.84$ μm and $\Lambda_2 = 154.96$ μm, respectively. The ratio of these two periods is $\Lambda_2/\Lambda_1 = 6$ and the duty cycle is 0.5, as is shown in Fig. 1. (More details about the selecting process could be referred to the **Methods** section).

To give a quantum mechanics description of our tunable entangled photon-pair source, we derive the state vector of entangled photons through the effective Hamiltonian. The total interaction Hamiltonian consists of two parts, which is expressed as $H_I = H_{SPDC} + H_{EO}$. H_{SPDC} corresponds to the SPDC processes, while H_{EO} refers to the EO interaction. Both of them arise from polarization, namely, P_{NL} and P_{EO}. In detailed treatments, the pump field is usually treated as an undepleted classical wave. The signal and idler fields are quantized and represented by field operators. Thus the formulations of the pump, signal and idler fields could be written as

$$E_p^{(+)} = E_{po}\vartheta_{po}(\vec{r})e^{i(\beta_{po}x-\omega_p t)}$$
$$E_s^{(-)} = i\sum_\sigma \int d\omega_s \sqrt{\frac{\hbar\omega_s}{2\varepsilon_0 n_{s\sigma}^2 N_{s\sigma}}}\vartheta_{s\sigma}(\vec{r})a_{s\sigma}^\dagger e^{-i(\beta_{s\sigma}x-\omega_s t)}, \quad (10)$$
$$E_i^{(-)} = i\sum_\sigma \int d\omega_i \sqrt{\frac{\hbar\omega_i}{2\varepsilon_0 n_{i\sigma}^2 N_{i\sigma}}}\vartheta_{i\sigma}(\vec{r})a_{i\sigma}^\dagger e^{-i(\beta_{i\sigma}x-\omega_i t)}$$

where σ represents the polarization state *o* or *e*, and $n_{j\sigma}$ (j = s, i) is the corresponding refractive index. $N_{s\sigma}$ and $N_{i\sigma}$ are normalization parameters. $\vartheta_{po}(r)$, $\vartheta_{s\sigma}(r)$ and $\vartheta_{i\sigma}(r)$ correspond to the transverse mode profiles of pump, signal and idler field, respectively.

For SPDC processes, if using the rotating wave approximation, H_{SPDC} is derived as

$$\begin{aligned} H_{SPDC} &= \frac{1}{2}\int_V d^3r P_{NL}\cdot E = \varepsilon_0 \int_V d^3r d(x) E_p^{(+)} E_s^{(-)} E_i^{(-)} + H.C. \\ &= -\frac{\hbar E_{po}}{2}\sum_{m,n} d_{31} G_{m,n}\Big[\int_{-L}^{0} dx e^{i(\beta_{po}-\beta_{so}-\beta_{ie}+K_{m,n})x} \\ &\times \iint d\omega_s d\omega_i F_{oe}\sqrt{\frac{\omega_s\omega_i}{n_{so}^2 n_{ie}^2 N_{so}N_{ie}}} a_{so}^\dagger a_{ie}^\dagger e^{-i(\omega_p-\omega_s-\omega_i)t} \\ &+ \int_{-L}^{0} dx e^{i(\beta_{po}-\beta_{se}-\beta_{io}+K_{m,n})x} \iint d\omega_s d\omega_i F_{eo}\sqrt{\frac{\omega_s\omega_i}{n_{se}^2 n_{io}^2 N_{se}N_{io}}} \\ &\times a_{se}^\dagger a_{io}^\dagger e^{-i(\omega_p-\omega_s-\omega_i)t} + H.C.\Big] \end{aligned} \quad (11)$$

with

$$\begin{aligned} F_{oe} &= \iint dydz\vartheta_{po}(\vec{r})\vartheta_{so}(\vec{r})\vartheta_{ie}(\vec{r}) \\ F_{eo} &= \iint dydz\vartheta_{po}(\vec{r})\vartheta_{se}(\vec{r})\vartheta_{io}(\vec{r}) \end{aligned} \quad (12)$$

For the EO process, the interaction Hamiltonian is derivate as above. H_{EO} is expressed as

$$\begin{aligned} H_{EO} = \frac{\hbar\varepsilon_0}{4}\sum_{m,n}\gamma_{51}E_a G_{m,n}\Big[\int_{-L}^{0} dx e^{i(\beta_{s'e}-\beta_{so}+K_{m,n})x} \\ \iint d\omega_s d\omega_{s'} F_{EO}\sqrt{\frac{\omega_s\omega_{s'}n_{so}^2 n_{s'e}^2}{N_{so}N_{s'e}}} a_{so}^\dagger a_{s'e} e^{-i(\omega_s-\omega_{s'})t} + \\ \int_{-L}^{0} dx e^{i(\beta_{so}-\beta_{s'e}+K_{m,n})x} \\ \iint d\omega_s d\omega_{s'} F_{EO}\sqrt{\frac{\omega_s\omega_{s'}n_{so}^2 n_{s'e}^2}{N_{so}N_{s'e}}} a_{s'e}^\dagger a_{so} e^{-i(\omega_{s'}-\omega_s)t}\Big] \end{aligned} \quad (13)$$

with

$$F_{EO} = \iint dydz\vartheta_{so}(\vec{r})\vartheta_{se}(\vec{r}) \quad (14)$$

The entangled state vector could be obtained through $|\Psi(t)\rangle = \exp[(-i/\hbar)\int dt(H_{SPDC}+H_{EO}(E_a))]|0\rangle$. Detailed treatments thus could be divided into two cases:

i) when there is no applied voltage, we expand the evolution operator to the first-order perturbation, so the state vector is expressed as

$$\begin{aligned} |\Psi\rangle &= [1-\frac{i}{\hbar}\int_{-\infty}^{\infty} dt H_{SPDC}(t)]|0\rangle \\ &= |0\rangle + \frac{iE_{po}}{2}\sum_{m,n} d_{31}G_{m,n}\iint d\omega_s d\omega_i [F_{oe}\sqrt{\frac{\omega_s\omega_i}{n_{so}^2 n_{ie}^2 N_{so}N_{ie}}}\int_{-L}^{0} dx e^{i(\beta_{po}-\beta_{so}-\beta_{ie}+K_{m,n})x} \\ &\times \int_{-\infty}^{\infty} dt e^{-i(\omega_p-\omega_s-\omega_i)t} a_{so}^\dagger a_{ie}^\dagger + F_{eo}\sqrt{\frac{\omega_s\omega_i}{n_{se}^2 n_{io}^2 N_{se}N_{io}}}\int_{-L}^{0} dx e^{i(\beta_{po}-\beta_{se}-\beta_{io}+K_{m,n})x} \\ &\times \int_{-\infty}^{\infty} dt e^{-i(\omega_p-\omega_s-\omega_i)t} a_{se}^\dagger a_{io}^\dagger]|0\rangle \end{aligned} \quad (15)$$

In the equation, we have $\int dt e^{-i(\omega_p-\omega_s-\omega_i)t} = 2\pi\delta(\omega_p-\omega_s-\omega_i)$ and $\int dx e^{i\Delta\beta x} = h(L\Delta\beta)$ with the formation $h(x) = e^{-ix/2}sinc(x/2)$. Moreover, the actual SPDC process doesn't merely arise at the perfect phase-matching frequencies Ω_s and Ω_i. As the natural bandwidth is ν, we set $\omega_s = \Omega_s + \nu$ and $\omega_i = \Omega_i - \nu$, then the state vector is simplified as

$$\begin{aligned} |\Psi\rangle &= |0\rangle + \int d\nu P_{oe} h(L\Delta\beta_{ooe}) a_{so}^\dagger a_{ie}^\dagger |0\rangle \\ &+ \int d\nu P_{eo} h(L\Delta\beta_{oeo}) a_{se}^\dagger a_{io}^\dagger |0\rangle \end{aligned} \quad (16)$$

with

$$\begin{aligned} P_{oe} &= i\pi L E_{po} d_{31} G_{3,1} F_{oe}\sqrt{\frac{\Omega_s\Omega_i}{n_{so}^2 n_{ie}^2 N_{so}N_{ie}}} \\ P_{eo} &= i\pi L E_{po} d_{31} G_{3,-1} F_{eo}\sqrt{\frac{\Omega_s\Omega_i}{n_{se}^2 n_{io}^2 N_{se}N_{io}}} \end{aligned} \quad (17)$$

In the equation, the phase mismatch terms could be expressed as $\Delta\beta_{ooe} = \beta_{p,o} - \beta_{s,o} - \beta_{i,e}$ and $\Delta\beta_{oeo} = \beta_{p,o} - \beta_{s,e} - \beta_{i,o}$. As $|\nu| \ll \Omega_s, \Omega_i$, we have substituted $\omega_s(\omega_i)$ by $\Omega_s(\Omega_i)$ in P_{oe} and P_{eo}.

ii) For the second case, the voltage E_a is applied. The evolution operator should be expanded to the second-order term. The formulation of the state vector could be expressed as

$$\begin{aligned} |\Psi\rangle &= [1+(-\frac{i}{\hbar})^2\int_{-\infty}^{\infty} dt_2\int_{-\infty}^{\infty} dt_1 T(H_{EO}(t_2)H_{SPDC}(t_1))]|0\rangle \\ &= |0\rangle + \frac{\varepsilon_0 d_{31}\gamma_{51}E_{po}E_a L^2}{8}\{\iint d\omega_s d\omega_{s'}\int_{-\infty}^{\infty} dt_2 e^{-i(\omega_s-\omega_{s'})t_2} F_{EO}[G_{1,1}h(L\Delta\beta_{eo})\sqrt{\frac{\omega_s\omega_{s'}n_{so}^2 n_{s'e}^2}{N_{so}N_{s'e}}} a_{so}^\dagger a_{s'e} \\ &+ G_{1,1}h(L\Delta\beta_{oe})\sqrt{\frac{\omega_s\omega_{s'}n_{so}^2 n_{s'e}^2}{N_{so}N_{s'e}}} a_{s'e}^\dagger a_{so}]\}\{\iint d\omega_s d\omega_i\int_{-\infty}^{\infty} dt_1 e^{-i(\omega_p-\omega_s-\omega_i)t_1} \\ &\times [G_{3,1}h(L\Delta\beta_{ooe})F_{oe}\sqrt{\frac{\omega_s\omega_i}{n_{so}^2 n_{ie}^2 N_{so}N_{ie}}} a_{so}^\dagger a_{ie}^\dagger + G_{3,-1}h(L\Delta\beta_{oeo})F_{eo}\sqrt{\frac{\omega_s\omega_i}{n_{se}^2 n_{io}^2 N_{se}N_{io}}} a_{se}^\dagger a_{io}^\dagger]\}|0\rangle \end{aligned} \quad (18)$$

In the equation, T is the time-ordering operator. The notation $\Delta\beta_{oe}$ corresponds to the mismatch of $\beta_{s,o}$ and $\beta_{s,e}$. The functions $h(L\Delta\beta_{ooe})$ and $h(L\Delta\beta_{oeo})$ are spatial integration for SPDC, while $h(L\Delta\beta_{oe})$ and $h(L\Delta\beta_{eo})$ correspond to the EO processes. There are four product terms of effective operators, including $a_{so}^\dagger a_{se} a_{se}^\dagger a_{io}^\dagger$, $a_{se}^\dagger a_{so} a_{so}^\dagger a_{ie}^\dagger$, $a_{so}^\dagger a_{se} a_{so}^\dagger a_{ie}^\dagger$ and $a_{se}^\dagger a_{so} a_{se}^\dagger a_{io}^\dagger$. The first two correspond to actual processes. If they act on the vacuum state, the results show $a_{so}^\dagger a_{se} a_{se}^\dagger a_{io}^\dagger|0\rangle = \left(a_{so}^\dagger|0_{so}\rangle\right)\left(a_{se}a_{se}^\dagger|0_{se}\rangle\right)\left(a_{io}^\dagger|0_{io}\rangle\right) = |1_{so},0_{se},1_{io}\rangle$ and $a_{se}^\dagger a_{so} a_{so}^\dagger a_{ie}^\dagger|0\rangle = \left(a_{se}^\dagger|0_{se}\rangle\right)\left(a_{so}a_{so}^\dagger|0_{so}\rangle\right)\left(a_{ie}^\dagger|0_{ie}\rangle\right) = |1_{se},0_{so},1_{ie}\rangle$. For the last two terms, they don't affect the final entangled state because as $a_{se}|0\rangle = 0$ and $a_{so}|0\rangle = 0$. Therefore the parallel-polarization entangled state is written as

$$\begin{aligned} |\Psi\rangle &= |0\rangle + \int d\nu\int d\nu' P_{oo} h(L\Delta\beta_{eo}) h(L\Delta\beta_{oeo}) a_{so}^\dagger a_{io}^\dagger |0\rangle \\ &+ \int d\nu\int d\nu' P_{ee} h(L\Delta\beta_{oe}) h(L\Delta\beta_{ooe}) a_{se}^\dagger a_{ie}^\dagger |0\rangle \end{aligned} \quad (19)$$

with

$$P_{oo}=\frac{\pi^2\varepsilon_0^2}{2}d_{31}\gamma_{51}\Omega_s E_{po}E_a G_{1,\,1}G_{3,\,-1}F_{EO}F_{eo}L^2\sqrt{\frac{n_{so}^2\Omega_s\Omega_i}{n_{io}^2N_{se}^2N_{io}N_{so}}}$$
$$P_{ee}=\frac{\pi^2\varepsilon_0^2}{2}d_{31}\gamma_{51}\Omega_s E_{po}E_a G_{1,\,1}G_{3,\,1}F_{EO}F_{oe}L^2\sqrt{\frac{n_{se}^2\Omega_s\Omega_i}{n_{ie}^2N_{so}^2N_{ie}N_{se}}} \quad (20)$$

Similarly, we also set $\omega_s=\Omega_s+v$ and $\omega_i=\Omega_i-v$, while ω_s (ω_i) is substituted by Ω_s (Ω_i) in P_{oo} and P_{ee}. Summarizing the two situations above, we rewrite the entangled state vector in a terser formation:

$$\begin{aligned}|\Psi\rangle=|0\rangle+(\int_{0-}^{0+}\delta(E_a)dE_a)[\int dvP_{oe}h(L\Delta\beta_{ooe})a_{so}^{\dagger}a_{ie}^{\dagger}|0\rangle\\ +\int dvP_{eo}h(L\Delta\beta_{oeo})a_{se}^{\dagger}a_{io}^{\dagger}|0\rangle]+(1-\int_{0-}^{0+}\delta(E_a)dE_a)\\ \times[\int dv\int dv'P_{oo}h(L\Delta\beta_{eo})h(L\Delta\beta_{oeo})a_{so}^{\dagger}a_{io}^{\dagger}|0\rangle\\ +\int dv\int dv'P_{ee}h(L\Delta\beta_{oe})h(L\Delta\beta_{ooe})a_{se}^{\dagger}a_{ie}^{\dagger}|0\rangle]\end{aligned} \quad (21)$$

In the equation, $\delta(E_a)$ represents the Dirac-δ function. When $E_a=0$, we have $\int_{0-}^{0+}\delta(E_a)dE_a=1$. The generated entangled state corresponds to $C_{oe}|o\rangle_s|e\rangle_i+C_{eo}|e\rangle_s|o\rangle_i$. If E_a is an appropriate nonzero value, the value of $(1-\int_{0-}^{0+}\delta(E_a)dE_a)$ should be 1, the entangled state vector is $C_{oo}|o\rangle_s|o\rangle_i+C_{ee}|e\rangle_s|e\rangle_i$. To ensure the EO transformation of the downconverted photons, several calculations have been done. The crystal length is set at 3 cm, and the average pump power is set at 1 W. Based on the coupled wave equations for EO interaction[16] and those for downconversion process, we obtain that when E_a is 3.8×10^5 V/m (Usually, the distance between the electrodes used for the LN waveguide is $10\sim1000$ μm, the corresponding applied voltage is about $1\sim100$ V)[35], the transformation efficiencies are $P_{se}/(P_{se}+P_{so})=0.9927$ (for $|o\rangle_p\rightarrow|o\rangle_s|e\rangle_i\rightarrow|e\rangle_s|e\rangle_i$) and $P_{so}/(P_{se}+P_{so})=0.9932$ (for $|o\rangle_p\rightarrow|e\rangle_s|o\rangle_i\rightarrow|o\rangle_s|o\rangle_i$), respectively. As for the idler photon, the polarization state is hardly rotated. That's because the PPLN's EO effect is quite special with wavelength selectivity. Only lights at the designed discrete wavelengths are affected. The corresponding wavelength bandwidth also could be predesigned. For a direct verification, the transformation efficiency of polarization of the idler photon is calculated to be about 1%. Therefore the corresponding influence could be neglected. The orthogonally polarized entangled pair could be transformed into parallel polarized entangled pair with a near 100% efficiency. Therefore EO tunable entangled states are realized. Furthermore, due to the intrinsic properties of EO modulation, the entangled state is fast switchable. That could be realized in both CW and pulsed pump regimes. In the CW pump regime, we could just set the voltage at a certain value until different output photon states are requested. For a 3-cm long sample, the switching time is limited by the propagation time from the entry to the exit surface, which is about 0.2 ns. Being different from the CW pump, the pulsed regime may give some more constrains. We should avoid changing the voltage when the pumped pulses propagate right in the sample. Since the highest repetition rate of commercial lasers are only around 100 MHz, the time gap between cascading pulses should be long enough for EO switching.

Characterization of the tunable entangled photon-pair source. To ensure the quality of our tunable entangled photon-pair source, we investigate the corresponding properties. Firstly, the spectrum character is discussed, which is represented by the modulus squares of h-functions. For type-II-like polarization entangled photons, the corresponding expressions are $|h(L\Delta\beta_{ooe})|^2$ and $|h(L\Delta\beta_{oeo})|^2$; while those for the type-I-like polarization entangled photons are simultaneously affected by SPDC process and EO interaction, so the formulations are $|h(L\Delta\beta_{eo})h(L\Delta\beta_{oeo})|^2$ and $|h(L\Delta\beta_{oe})h(L\Delta\beta_{ooe})|^2$, respectively. Calculation results are presented in Fig. 2. The natural spectral bandwidth of entangled **photon-pair** source is mainly influenced by the group velocities of the signal and idler wavelengths. In our situation, these two wavelengths are close with each other, so the differences between the bandwidths for the two SPDC processes, *i. e.*, $o_p\rightarrow o_s+e_i$, $o_p\rightarrow e_s+o_i$ are relatively small. From Fig. 2(a) and Fig. 2(b), when the waveguide length L is 3 cm, these two quantities are 0.35 nm and 0.27 nm, respectively. Compared with the previous report[30], these values are relatively smaller, which is beneficial to the improvement of entanglement degree. On the other hand, the natural bandwidth increases with the decrease of the waveguide length L. For instance, we could see that the value of bandwidth increase to ~0.9 nm for $o_p\rightarrow o_s+e_i$ process when the crystal length reduces to 1 cm. For $C_{oo}|o\rangle_s|o\rangle_i+C_{ee}|e\rangle_s|e\rangle_i$ pairs, as the EO process is integrated together, the natural bandwidths are further restricted through the corresponding h-functions. If the waveguide length L is 3 cm, the bandwidths for ordinary and extraordinary photon pairs are 0.20 nm and 0.23 nm, respectively. The difference between these two values is smaller, and the spectrum is almost symmetrical.

The anticorrelation dip could be calculated based on the spectrum function, which is usually different for type-I and type-II SPDC[36]. It is the Fourier transform of the SPDC spectrum. The corresponding formulation is $R_C(\tau)\sim1-(1/2\pi)\int|h(v)|^2\cos(v\tau)dv$. A narrower dip corresponds to a broader spectrum, so the width of anticorrelation dip is mainly determined by the natural bandwidth of the SPDC spectrum. For the orthogonally polarized entangled pair, $|h(v)|^2$ corresponding to $sinc^2(L\Delta\beta_{ooe}/2)$ and $sinc^2(L\Delta\beta_{oeo}/2)$. We expand the phase mismatching to the first nonzero order of v. The corresponding formulations are $\Delta\beta_{ooe}\approx-(\beta_{so}'-\beta_{ie}')v$ and $\Delta\beta_{oeo}\approx-(\beta_{se}'-\beta_{io}')v$. $\beta_{j\sigma}'$ (j = p, s, i; σ = o, e) represents the dispersion parameter. For the parallel polarized entangled pair, as its spectrum is further confined by EO process, the spectrum property is naturally different from those of the traditional cases. The $|h(v)|^2$ functions are written as $sinc^2(L\Delta\beta_{ooe}/2)\cdot sinc^2(L\Delta\beta_{oe}/2)$ and $sinc^2(L\Delta\beta_{oeo}/2)\cdot sinc^2(L\Delta\beta_{eo}/2)$. Similarly, we have $\Delta\beta_{oe}\approx(\beta_{so}'-\beta_{se}')v$ and $\Delta\beta_{eo}\approx(\beta_{se}'-\beta_{so}')v$. As an illustration, the anticorrelation dips corresponding to $sinc^2(L\Delta\beta_{ooe}/2)$ and $sinc^2(L\Delta\beta_{ooe}/2)\cdot sinc^2(L\Delta\beta_{oe}/2)$ are plotted in Fig. 3.

Based on the discussions above, we calculate the von Neumann entropy of our source, in which the influences of $P_{k\delta}$ (k, δ = o, e) are included. It is defined as $S=-tr(\rho_{sub}\log_2\rho_{sub})$[37]. ρ_{sub} represents the reduced density operator for the subsystems. For a product state, the quantity vanishes. If the state is maximally entangled, the value of the entropy is 1. To describe tunable entangled **photon-pair** source, the density operator of the entangled state is expressed as follows

$$\hat{\rho}_{si}=\left(\int_{0-}^{0+}\delta(E_a)dE_a\right)|\varphi_{\rm O}\rangle\langle\varphi_{\rm O}|+\left(1-\int_{0-}^{0+}\delta(E_a)dE_a\right)|\phi_{\rm P}\rangle\langle\phi_{\rm P}| \quad (22)$$

with

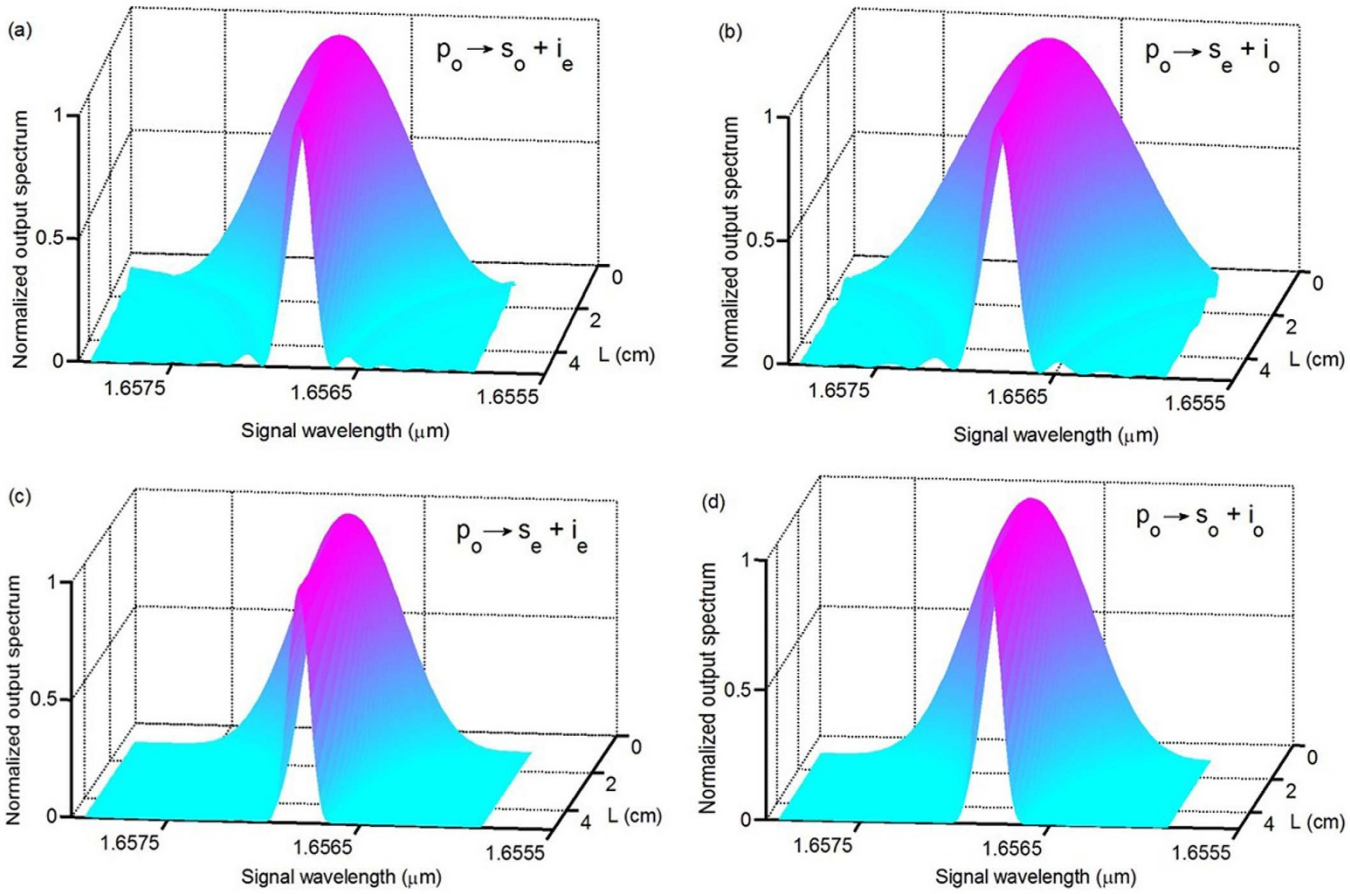

Figure 2 | Normalized output signal spectra corresponding to the two type of entangled states, respectively. (a) $o_p \rightarrow o_s + e_i$; (b) $o_p \rightarrow e_s + o_i$; (c) $o_p \rightarrow o_s + e_i \rightarrow e_s + e_i$; (d) $o_p \rightarrow e_s + o_i \rightarrow o_s + o_i$. The corresponding natural bandwidths are 0.27 nm, 0.35 nm, 0.20 nm and 0.23 nm, when the waveguide length L is 3 cm.

$$
\begin{aligned}
|\varphi_O\rangle &= \int dv P_{oe} h(L\Delta\beta_{ooe}) a^{\dagger}_{so} a^{\dagger}_{ie} |0\rangle + \int dv P_{eo} h(L\Delta\beta_{oeo}) a^{\dagger}_{se} a^{\dagger}_{io} |0\rangle \\
|\phi_P\rangle &= \int dv \int dv' P_{oo} h(L\Delta\beta_{eo}) h(L\Delta\beta_{oeo}) a^{\dagger}_{so} a^{\dagger}_{io} |0\rangle \\
&+ \int dv \int dv' P_{ee} h(L\Delta\beta_{oe}) h(L\Delta\beta_{ooe}) a^{\dagger}_{se} a^{\dagger}_{ie} |0\rangle
\end{aligned}
\tag{23}
$$

The reduced density operator could be obtained through $\hat{\rho}_s = -tr_i(\hat{\rho}_{si})$. Therefore the quantity S is derived as

$$
\begin{aligned}
S = &-\left(\int_{0-}^{0+} \delta(E_a) dE_a\right) \left[\frac{\Theta_{oe}}{\Theta_O} \log_2\left(\frac{\Theta_{oe}}{\Theta_O}\right) + \frac{\Theta_{eo}}{\Theta_O} \log_2\left(\frac{\Theta_{eo}}{\Theta_O}\right)\right] \\
&-\left(1 - \int_{0-}^{0+} \delta(E_a) dE_a\right) \left[\frac{\Theta_{oo}}{\Theta_P} \log_2\left(\frac{\Theta_{oo}}{\Theta_P}\right) + \frac{\Theta_{ee}}{\Theta_P} \log_2\left(\frac{\Theta_{ee}}{\Theta_P}\right)\right]
\end{aligned}
\tag{24}
$$

where $\Theta_{oe} = \left|\int dv P_{oe} h(L\Delta\beta_{ooe})\right|^2$, $\Theta_{eo} = \left|\int dv P_{eo} h(L\Delta\beta_{oeo})\right|^2$, $\Theta_{oo} = \left|\int dv \int dv' P_{oo} h(L\Delta\beta_{eo}) h(L\Delta\beta_{oeo})\right|^2$ and $\Theta_{ee} = \left|\int dv \int dv' P_{ee} h(L\Delta\beta_{oe}) h(L\Delta\beta_{ooe})\right|^2$. Besides, $\Theta_O = \Theta_{oe} + \Theta_{eo}$ and $\Theta_P = \Theta_{oo} + \Theta_{ee}$.

From the equation above, we could see that the value of S is mainly determined by Θ_{ij} (i, j = o, e). In an ideal situation, *i.e.*, $\Theta_{oe} = \Theta_{eo}$ and $\Theta_{oo} = \Theta_{ee}$, S would reach its maximal value 1, which corresponds to the maximal entanglement. If the natural bandwidth is narrow, and the ratio P_{oe}/P_{eo}, P_{oo}/P_{ee} is close to 1, Θ_{oe} and Θ_{oo} thus are almost equal to Θ_{eo} and Θ_{ee}, which makes $S \approx 1$ and a very high degree of entanglement. On the contrary, wider bandwidth would affect the entanglement accordingly. As is discussed above, the natural bandwidth in our case is quite small. Following the treatments in Ref. 38, we simplify the calculation of S into the perfect phase matching situation. Thus S has the same formulation for two types of entangled states. This result verifies that EO process does not affect

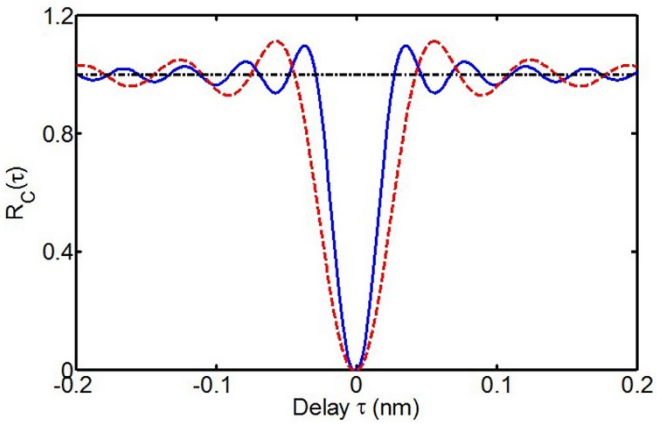

Figure 3 | The anticorrelation dips Rc(τ) are calculated based on $sinc^2(L\Delta\beta_{ooe}/2)$ and $sinc^2(L\Delta\beta_{ooe}/2) \times sinc^2(L\Delta\beta_{oe}/2)$, respectively. The blue solid line corresponds to the former, while the red dashed line represents the latter one. The crystal length is set at 3 cm.

the entanglement degree. Besides, we could see that $P_{k\delta}$ is mainly influenced by geometry and material parameters from Eq. (21). We find that the source has high tolerance for the geometrical variations. Until the waveguide modes of λ_s and λ_i are nearly cutoff, S still stays above 0.99. The degree of entanglement maintains in a high level.

Discussion

What we have presented above is merely a simplest case for the two-photon entangled state, where the entangled states are generated and manipulated through EO modulation. Moreover, this type of system also could be used to generate multiphoton entanglement. A straightforward proposal is considered based on the switchable two-photon entanglement source proposed above. For our device, if the voltage is turned on, the generated entangled state would be $|ee\rangle + |oo\rangle$. We may increase the pump power to improve the simultaneous generation possibility of double photon pairs in SPDC processes. In this situation, we may obtain four states with the same possibility, namely, $|ee\rangle|ee\rangle$, $|oo\rangle|oo\rangle$, $|ee\rangle|oo\rangle$ and $|oo\rangle|ee\rangle$. To demonstrate the entanglement, we'd better erase influences of $|ee\rangle|oo\rangle$ and $|oo\rangle|ee\rangle$. That could be realized through a post-selected detection scheme, which is widely used in energy-time entanglement. After the generated photon pairs pass through a single domain LN waveguide, the arrival time of o-polarized and e-polarized photons would be different due to the birefringence. If the frequencies of the down-converted photons are close and chosen around telecom band, the frequency dispersion would be small enough to be neglected[39]. Therefore $|ee\rangle|ee\rangle$ and $|oo\rangle|oo\rangle$ could be detected the same time, while there would be time difference in detection of photons in $|ee\rangle|oo\rangle$ and $|oo\rangle|ee\rangle$ states. With a narrow time window that is usually used in energy-time entanglement[40], a four-photon GHZ state could be selected and detected. Moreover, with the help of on-chip optical elements, such as, mode analyzer, directional coupler, Mach–Zehnder interferometer and Y-coupler[19,22,39], entangled state of more than four photons and preselected entanglement scheme are designable.

Moreover, with the help of artificially designed domain structures, the nonmaximally entangled state[3,5] could also be easily realized, which can find applications in the loophole-free tests of Bell inequalities[41] and quantum metrology with the presence of photon loss[42]. The LN waveguide could be divided into several functional portions along the propagation direction[19,22]. We may set the first portion to regulate the amplitude ratio of o-polarized and e-polarized pump light through EO interaction. Since both the o-polarized and e-polarized pump lights are involved, two corresponding SPDC processes, namely, $o_p \rightarrow o_s + o_i$ and $e_p \rightarrow e_s + e_i$ may happen simultaneously in the second portion. They are dominated by the nonlinear coefficients d_{22} and d_{33}, respectively. In this case, the QPM conditions also could be satisfied for these two processes through suitable domain design. The non-maximally entangled state thus could be obtained that is expressed as $|o_s,o_i\rangle + \varepsilon|e_s,e_i\rangle$. The relative ratio ε of amplitude may be controlled by the voltage applied on the first portion. As a consequence, an EO tunable non-maximally entanglement source is realized. The mixed state entanglement is not hard to be generated based on nonmaximal entanglement. A usual procedure is to create an entangled state with desired degree of entanglement, modulate the density matrix and then introduce decoherence[6,7]. The first step could be realized through non-maximal entanglement with a suitable entanglement degree, and then we could utilize the EO polarization rotation effect to modulate the non-maximally entangled state to generate off-diagonal terms in the corresponding density matrix. To introduce decoherence into the system, experiments using bulk optical elements have been demonstrated based on the spacial properties of the SPDC emission cone[6,7]. However, in waveguide systems, it's not convenient to use spatial decoherence directly. We could consider the temporal decoherence. Through introducing birefringent retardation, the vector $|oe\rangle$ and $|eo\rangle$ could be distinguished from $|oo\rangle$ and $|ee\rangle$ via the relative arrival time difference between two photons. Tracing over time, coherence between distinguishable terms in the density matrix could be erased, thus specific off-diagonal terms become smaller to form the target mixed entangled state.

It's worth mentioning that besides the uniform domain periods we used all above, the domain structure of LN or similar materials could be elaborately prepared in more complicated patterns, such as quasi-periodic structures, which could provide complex reciprocal vectors to compensate the multi-process phase mismatching with high efficiency[43]. We believe the domain engineered nonlinear waveguide is really a very promising platform for quantum integration circuits, which deserves more in-depth studies in both theories and experiments[44].

As for practical applications of our device, the quantum cryptography protocol may be a potential area, which is the most realizable quantum information application nowadays[45]. Based on the fast switching entangled state, our device provides a different strategy for quantum cryptography. Instead of switching the complementary analysis basis at the users' (Alice and Bob) places, we could switch between the states directly at the source while keeping the analysis basis always oriented along the same direction. Although this strategy may cause certain constrains, an advantage is that the operation conveniences for users may be improved. Another possible application example would be the classical and quantum communication without a shared reference frame[46]. Alice may encode a logical qubit as $|0_L\rangle = (|HH\rangle + |VV\rangle)/\sqrt{2}$, $|1_L\rangle = (|HV\rangle + |VH\rangle)/\sqrt{2}$, and use it to communicate with Bob. If one applies a rotation to both of the photons, $|0_L\rangle$ is unchanged, *i.e.*, it is invariant under arbitrary rotations of the reference frame around the propagation axis. Although $|1_L\rangle$ will be changed, it is still orthogonal to $|0_L\rangle$. Therefore without a shared reference frame or the pre-alignment of Alice and Bob's polarization basis, a projective measurement on $|0_L\rangle$ by Bob will distinguish the two logical bases. Furthermore, with small postprocessing modifications based on on-chip optical elements mentioned above[19,22,39], our source can switch between the generation of two entangled states with different symmetries $(|HH\rangle + |VV\rangle)/\sqrt{2}$ and $(|HV\rangle - |VH\rangle)/\sqrt{2}$, both of which are invariant under the rotation of the reference frame[47]. Thus a symmetry measurement by Bob will distinguish between the two states. The similar idea can also be applied to the error correction protocol in quantum computations. Moreover, in most of the integrated platforms to date, the quantum information is encoded in the spatial modes[24–26]. Manipulating the polarization of photons on chip allows us to encode and decode classical and quantum information in the polarization degree of

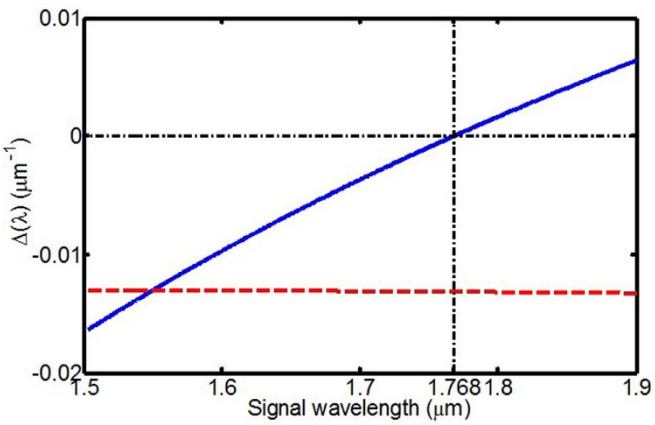

Figure 4 | The values of $\Delta(\lambda)$ against the signal wavelengths when λ_p is equal to 775 nm. The blue solid line corresponds to $(m_3, n_3) = (1, 1)$, while the red dash line corresponds to $(m_3, n_3) = (1, -1)$. Only the blue line has crossover point with the zero line, so (1, 1) is possible solution for the equation $\Delta(\lambda) = \Delta\beta_3(\lambda) - G_{1,\pm 1} = 0$.

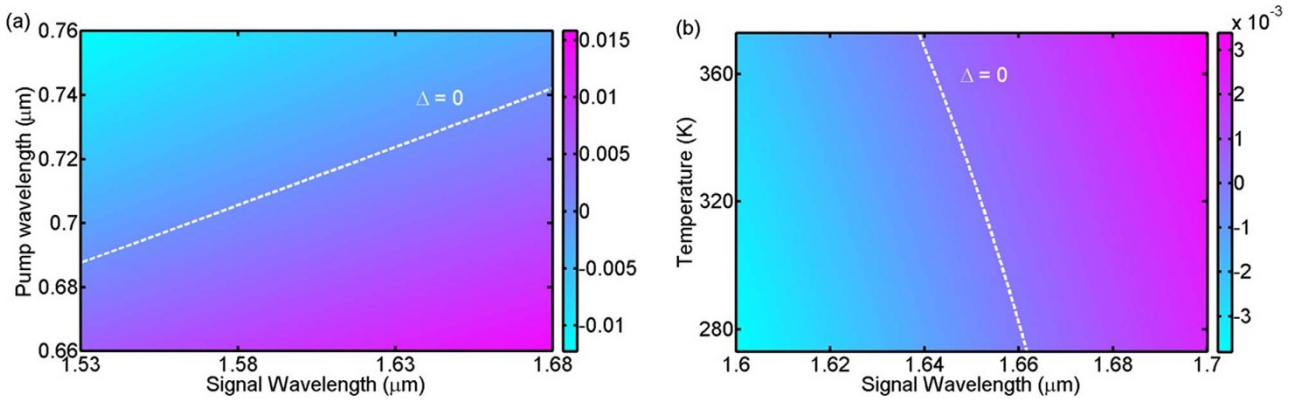

Figure 5 | In the situation where the subscript of $\Delta\beta_3$ corresponds to $(m_3, n_3) = (1, 1)$, The function $\Delta(\lambda)$ is tuned by the pump wavelength and the operation temperature, respectively. The green dashed line marks $\Delta(\lambda) = 0$. (a) Values of $\Delta(\lambda)$ change with the signal wavelengths and the pump wavelengths. (b) Values of $\Delta(\lambda)$ changes with the signal wavelengths and the operation temperature. From the $\Delta(\lambda) = 0$ lines, suitable pairs of pump, signal and idler wavelengths could be chosen for specific situations.

freedom. Fast switching means the shorter operation time of qubit, which is a desirable feature in practical applications. We believe over 1 GHz modulation bandwidth would be easily achieved in this case.

In summary, we theoretically propose an effective approach to tailoring entangled photons through the combination of SPDC and EO effects. Based on the domain-engineered LN waveguide, an EO tunable polarization entangled photon-pair source is realized. It could selectively generate orthogonal-polarization or parallel-polarization photon by adjusting the applied voltage. The bandwidths and entanglement degrees of both types of entangled states are of excellent performances. In comparison with the bulk or in-fiber beam splitting, polarization handling, and wave plate elements, we proposed an integrated solution possibly on a single monolithic LN chip. This on-chip integration would be very desired in future quantum information related applications since it could be more compact, low loss and stable. In addition, the EO tunability is another attractive feature that supplies extremely fast manipulation on entangled photons, which is superior to the fixed wave plate solution. Moreover, the manipulation of some other entangled states are also discussed based on our proposals, including the multi-photon entangled state, the mixed entangled state and the nonmaximally entangled state, which show some attractive advantages. Introducing EO polarization modulation into domain engineered nonlinear waveguides offers opportunities for on-chip manipulation of quantum states and fast reconfigurability of the dedicated quantum chips, which is very desired for practical applications in future quantum circuits.

Methods

To find a proper set of pump, signal and idler wavelengths, they are scanned carefully. Firstly, when the pump wavelength is fixed, calculation results reveal that $\Delta\beta_1$ and $\Delta\beta_2$ (for SPDC processes) are close but much greater than $\Delta\beta_3$ (for EO interaction). Thus they are assumed to correspond to the solutions $(3, \pm 1)$ for (m, n), respectively. For certain pairs of signal and idler frequencies, the values of $\Lambda_1(\lambda)$ and $\Lambda_2(\lambda)$ could be calculated through linear superposition of $\Delta\beta_1(\lambda)$ and $\Delta\beta_2(\lambda)$, and then we compare the linear combination $(1, \pm 1)$ of $2\pi/\Lambda_1$ and $2\pi/\Lambda_2$ with $\Delta\beta_3$ to see if they are matched. The corresponding expression is $\Delta(\lambda) = \Delta\beta_3(\lambda) - G_{1,\pm 1}$. For the wavelength satisfying $\Delta(\lambda) = 0$, three phase mismatches could be compensated simultaneously.

In this study, we choose the pump wavelength at 775 nm. The values of $\Delta(\lambda)$ against the signal wavelengths are plotted in Fig. 4 ($\lambda_p = 775$ nm). It is seen from the figure that only the linear combination (1, 1) of $2\pi/\Lambda_1$ and $2\pi/\Lambda_2$ provides a solution for the equation $\Delta(\lambda) = 0$. Thus $G_{3,1}$ $G_{3,-1}$, $G_{1,1}$ are selected as the compensations of $\Delta\beta_1$, $\Delta\beta_2$ and $\Delta\beta_3$, respectively. Moreover, the phase matching conditions could be adjusted by the pump wavelength and the operation temperature, which are correspondingly shown in Fig. 5(a) and Fig. 5(b). To ensure the ratio between Λ_1 and Λ_2 is an integer, we finally choose the pump, signal and idler wavelengths at 0.7335 μm, 1.6568 μm and 1.3162 μm, respectively. In this situation, $\Lambda_2 = 6\Lambda_1$, where the operating temperature is set at 25°C. For quantum communication applications, the operation wavelengths might be preferred to be chosen from the telecom-band. That could be easily realized by finding the solutions of Eq. (9) accordingly, as is shown in Fig. 5(a). It is clearly from the figure that the whole telecom C band (1.53 μm–1.57 μm) and L band (1.57 μm–1.61 μm) could be selected for operation. Furthermore, the operating temperature could also be conveniently adjusted according the simulation results as shown in Fig. 5(b).

1. Eibl, M. *et al.* Experimental observation of four-photon entanglement from parametric down-conversion. *Phys. Rev. Lett.* **90**, 200403 (2003).
2. Zou, X. B. & Mathis, W. Generating a four-photon polarization-entangled cluster state. *Phys. Rev. A* **71**, 032308 (2005).
3. White, A. G., James, D. F., Eberhard, P. H. & Kwiat, P. G. Nonmaximally entangled states: Production, characterization, and utilization. *Phys. Rev. Lett.* **83**, 3103–3107 (1999).
4. Bennett, C. H., DiVincenzo, D. P., Smolin, J. A. & Wootters, W. K. Mixed-state entanglement and quantum error correction. *Phys. Rev. A* **54**, 3824–3851 (1996).
5. Thew, R. T., Tanzilli, S., Tittel, W., Zbinden, H. & Gisin, N. Experimental investigation of the robustness of partially entangled qubits over 11 km. *Phys. Rev. A* **66**, 062304 (2002).
6. Cinelli, C., di Nepi, G., de Martini, F., Barbieri, M. & Mataloni, P. Parametric source of two-photon states with a tunable degree of entanglement and mixing: Experimental preparation of Werner states and maximally entangled mixed states. *Phys. Rev. A* **70**, 022321 (2004).
7. Barbieri, M., de Martini, F., di Nepi, G. & Mataloni, P. Generation and characterization of Werner states and maximally entangled mixed states by a universal source of entanglement. *Phys. Rev. Lett.* **92**, 177901 (2004).
8. Kwiat, P. G., Waks, E., White, A. G., Appelbaum, I. & Eberhard, P. H. Ultrabright source of polarization-entangled photons. *Phys. Rev. A* **60**, R773–R776 (1999).
9. Leng, H. Y. *et al.* On-chip steering of entangled photons in nonlinear photonic crystals. *Nat. Commun.* **2**, 429 (2011).
10. Politi, A. *et al.* Integrated quantum photonics. *IEEE J. Sel. Top. Quantum Electron.* **15**, 1673–1684 (2009).
11. Tanzilli, S. *et al.* On the genesis and evolution of integrated quantum optics. *Laser & Photon. Rev.* **6**, 115–143 (2012).
12. Suhara, T. Generation of quantum-entangled twin photons by waveguide nonlinear-optic devices. *Laser & Photon. Rev.* **3**, 370–393 (2009).
13. de Chatellus, H. G., Sergienko, A. V., Saleh, B. E., Teich, M. C. & Di Giuseppe, G. Non-collinear and non-degenerate polarization-entangled photon generation via concurrent type-I parametric downconversion in PPLN. *Opt. Express* **14**, 10060–10072 (2006).
14. Bonneau, D. *et al.* Fast path and polarization manipulation of telecom wavelength single photons in lithium niobate waveguide devices. *Phys. Rev. Lett.* **108**, 053601 (2012).
15. Martin, A., Alibart, O., de Micheli, M. P., Ostrowsky, D. B. & Tanzilli1, S. A quantum relay chip based on telecommunication integrated optics technology. *New. J. Phys.* **14**, 025002 (2012).
16. Lu, Y. Q., Wan, Z. L., Wang, Q., Xi, Y. X. & Ming, N. B. Electro-optic effect of periodically poled optical superlattice LiNbO3 and its applications. *Appl. Phys. Lett.* **77**, 3719–3721 (2000).
17. Kaiser, F. *et al.* High-quality polarization entanglement state preparation and manipulation in standard telecommunication channels. *New. J. Phys.* **14**, 085015 (2012).
18. Herrmann, H. *et al.* Post-selection free, integrated optical source of non-degenerate, polarization entangled photon pairs. *Opt. Express* **21**, 27981–27991 (2013).

19. Lugani, J., Ghosh, S. & Thyagarajan, K. Electro-optically switchable spatial-mode entangled photon pairs using a modified Mach–Zehnder interferometer. *Opt. Lett.* **37**, 3729–3731 (2012).
20. Song, X. S., Yu, Z. Y., Wang, Q., Xu, F. & Lu, Y. Q. Polarization independent quasi-phase-matched sum frequency generation for single photon detection. *Opt. Express* **19**, 380–386 (2011).
21. Lu, Y. Q. *et al.* Optical properties of an ionic-type phononic crystal. *Science* **284**, 1822–1824 (1999).
22. Saleh, M. F., Di Giuseppe, G., Saleh, B. E. & Teich, M. C. Modal and polarization qubits in Ti:LiNbO3 photonic circuits for a universal quantum logic gate. *Opt. Express* **18**, 20475–20490 (2010).
23. Xu, P. *et al.* Lensless imaging by entangled photons from quadratic nonlinear photonic crystals. *Phys. Rev. A* **86**, 013805 (2012).
24. Politi, A., Cryan, M. J., Rarity, J. G., Yu, S. & O'Brien, J. L. Silica-on-silicon waveguide quantum circuits. *Science* **320**, 646–649 (2008).
25. Matthews, J. C., Politi, A., Stefanov, A. & O'Brien, J. L. Manipulation of multiphoton entanglement in waveguide quantum circuits. *Nat. photon.* **3**, 346–350 (2009).
26. Metcalf, B. J. *et al.* Multiphoton quantum interference in a multiport integrated photonic device. *Nat. commun.* **4**, 1356 (2013).
27. Sansoni, L. *et al.* Polarization entangled state measurement on a chip. *Phys. Rev. Lett.* **105**, 200503 (2010).
28. Crespi, A. *et al.* Integrated photonic quantum gates for polarization qubits. *Nat. Commun.* **2**, 566 (2011).
29. Sharma, A. & Bindal, P. Analysis of diffused planar and channel waveguides. *IEEE J. Quantum Electron.* **29**, 150–153 (1993).
30. Thyagarajan, K. *et al.* Generation of polarization-entangled photons using type-II doubly periodically poled lithium niobate waveguides. *Phys. Rev. A* **80**, 052321 (2009).
31. Gong, Y. X. *et al.* Compact source of narrow-band counterpropagating polarization-entangled photon pairs using a single dual-periodically-poled crystal. *Phys. Rev. A* **84**, 053825 (2011).
32. Lambda Photometrics Ltd., http://www.lambdaphoto.co.uk/pdfs/Inrad_datasheet_LNB.pdf (accessed 09/02/2014).
33. Volk, T. R. *et al.* Optical and non-linear optical investigations in $LiNbO_3$:Mg and $LiNbO_3$:Zn. *Ferroelectrics* **109**, 345 (1990).
34. Kumar, R. M. *et al.* SIMS-depth profile and microstructure studies of Ti-diffused Mg-doped near-stoichiometric lithium niobate waveguide. *J. Cryst. Growth* **287**, 472–477 (2006).
35. Huang, C. Y., Lin, C. H., Chen, Y. H. & Huang, Y. C. Electro-optic Ti:PPLN waveguide as efficient optical wavelength filter and polarization mode converter. *Opt. Express* **15**, 2548–2554 (2007).
36. Burlakov, A. V., Chekhova, M. V., Karabutova, O. A. & Kulik, S. P. Collinear two-photon state with spectral properties of type-I and polarization properties of type-II spontaneous parametric down-conversion: preparation and testing. *Phys. Rev. A* **64**, 041803(R) (2001).
37. Nielson, M. A. & Chuang, I. L. Quantum computation and quantum information. (Cambridge University Press, 2006).
38. Lugani, J. *et al.* Generation of modal- and path-entangled photons using a domain-engineered integrated optical waveguide device. *Phys. Rev. A* **83**, 062333 (2011).
39. Saleh, M. F., di Giuseppe, G., Saleh, B. E. A. & Teich, M. C. Photonic circuits for generating modal, spectral, and polarization entanglement. *IEEE Photon. J.* **2**, 736–752 (2010).
40. Tanzilli, S. *et al.* PPLN waveguide for quantum communication. *Eur. Phys. J. D* **18**, 155–160 (2002).
41. Giustina, M. *et al.* Bell violation using entangled photons without the fair-sampling assumption. *Nature* **497**, 227–230 (2013).
42. Dorner, U. *et al.* Optimal quantum phase estimation. *Phys. Rev. Lett.* **102**, 040403 (2009).
43. Zhu, S. N., Zhu, Y. Y. & Ming, N. B. Quasi-phase-matched third-harmonic generation in a quasi-periodic optical superlattice. *Science* **278**, 843–846 (1997).
44. Ming, Y. *et al.* Quantum entanglement based on surface phonon polaritons in condensed matter systems. *AIP Advances* **3**, 042122 (2013).
45. Martin, A. *et al.* Cross time-bin photonic entanglement for quantum key distribution. *Phys. Rev. A* **87**, 020301(R) (2013).
46. Bartlett, S. D. *et al.* Classical and quantum communication without a shared reference frame. *Phys. Rev. Lett.* **91**, 027901 (2003).
47. Aolita, L. *et al.* Quantum communication without alignment using multiple-qubit single-photon states. *Phys. Rev. Lett.* **98**, 100501 (2007).

Acknowledgments

The authors thank the helpful discussions with Dr. Li-jian Zhang for preparing the revised manuscript. This work is sponsored by 973 programs with contract No. 2011CBA00205 and 2012CB921803, and the National Science Fund for Distinguished Young Scholars with contract No. 61225026. The authors also thank the supports from PAPD and Fundamental Research Funds for the Central Universities. The technical support from Miss Ting-ting Xu is also acknowledged.

Author contributions

Y.Q.L. and Y.M. contributed to the original idea. Y.M., Z.J.W. and Z.X.C. did theoretical analysis, calculations and interpretations. A.H.T. provided theoretical guidance. Y.M. and Y.Q.L. wrote the manuscript together. Y.Q.L. and F.X. supervised the project. All authors reviewed the manuscript.

Additional information

Competing financial interests: The authors declare no competing financial interests.

How to cite this article: Ming, Y. *et al.* Tailoring entanglement through domain engineering in a lithium niobate waveguide. *Sci. Rep.* **4**, 4812; DOI:10.1038/srep04812 (2014).

This work is licensed under a Creative Commons Attribution-NonCommercial-ShareAlike 3.0 Unported License. The images in this article are included in the article's Creative Commons license, unless indicated otherwise in the image credit; if the image is not included under the Creative Commons license, users will need to obtain permission from the license holder in order to reproduce the image. To view a copy of this license, visit http://creativecommons.org/licenses/by-nc-sa/3.0/